The Performance Test of Different Horizontal Axis Wind Turbine (HAWT) Blade Shapes Using Experimental and Numerical Methods

P. Murathi Anil Kumar
M.Tech Student (Advanced Manufacturing System),
Sri Krishna Devaraya Engineering College,
NH-7 Gooty, Anantapur (Dist),
Andhra Pradesh -515401, India.

Dr. R. Ramachandra
Supervisor & Principal,
Sri Krishna Devaraya Engineering College,
NH-7 Gooty, Anantapur (Dist),
Andhra Pradesh -515401, India.

Abstract:

Three different horizontal axis wind turbine (HAWT) blade geometries with the same diameter of 0.72 m using the same NACA4418 airfoil profile have been investigated both experimentally and numerically. The first is an optimum (OPT) blade shape, obtained using improved blade element momentum (BEM) theory. A detailed description of the blade geometry is also given. The second is an untapered and optimum twist (UOT) blade with the same twist distributions as the OPT blade.

The third blade is untapered and untwisted (UUT). Wind tunnel experiments were used to measure the power coefficients of these blades, and the results indicate that both the OPT and UOT blades perform with the same maximum power coefficient, $Cp = 0.428$, but it is located at different tip speed ratio, $\lambda = 4.92$ for the OPT blade and $\lambda = 4.32$ for the UOT blade. The UUT blade has a maximum power coefficient of $Cp = 0.210$ at $\lambda = 3.86$. After the tests, numerical simulations were performed using a full three-dimensional computational fluid dynamics (CFD) method using the k-ω SST turbulence model.

It has been found that CFD predictions reproduce the most accurate model power coefficients. The good agreement between the measured and computed power coefficients of the three models strongly suggest that accurate predictions of HAWT blade performance at full-scale conditions are also possible using the CFD method.

Keywords:

Horizontal axis wind turbine; blade element momentum theory; wind tunnel experiment; power coefficient; computational fluid dynamics

1. Introduction:

For a horizontal-axis wind turbine (HAWT) system, the efficiency of the system transformation is related to the blade shape. Therefore it is critical to design the most efficient blade shape possible. Blade element momentum (BEM) theory is widely used when designing a HAWT blade shape and predicts its performance using a fairly simple procedure [1]. This theory requires combining the two-dimensional (2D) airfoil data to obtain the optimum blade shape, including the distributions of chord length and the twist angle along the span-wise direction. It should be noted that the optimization of a HAWT blade is done at the design tip speed ratio (λd) and the design angle of attack (αD). In other words, if the optimal blade is operated at a different tip speed ratio than the one for which it has been designed, it will no longer be optimal [1,2]. However, for this paper the performances of the blade are tested for the entire range between the tip speed ratios of 0 and 9. In past research, analysis focused only on the optimal blade shape within a constant-speed operation system [3–5]. The purpose of this study is to construct a HAWT system with variable-speed operation in which the optimum blade is determined using BEM theory. For comparative purposes, two other blades are also considered, as will be discussed later.

In general, three methods may be used to analyze the performance of HAWT blades. The first one is the improved BEM model, as performed by Bai et al. [6] and this model can quickly predict the blade performance. This improved BEM model includes two modifications that can greatly increase the accuracy for the blade performance curve prediction: tip-loss factor by Prandtl [7] and the stall delay model [8,9]. The second method is to experiment in a wind tunnel. For instances, Hirahara et al. [10] and Koki et al. [11] propose using the similitude method by measuring the mechanical torque generated by the blade using a small-scale wind turbine system. Both papers use a torque transducer installed on the shaft between the blade and the generator to measure the mechanical torque. Hirahara et al. [10] applied an electronic load to change the rotational speed of the rotor blade to obtain performance curves. This technique has been successfully applied to a 500 mm diameter 4-blade HAWT system that ran at a rated rotational speed of 1500 rpm and a rated wind speed of 12 m/s.

Here, the power coefficient (Cp), which is the efficiency transferred from the blade, was successfully calculated using a torque transducer. In addition, it was found that both the generator's efficiency and the system's total efficiency can be determined in this wind tunnel experiment. In a previous experiment, Koki et al. [11] used BEM theory to verify and compare the results with the performance curves of a wind tunnel experiment and found that BEM is a good method for predicting the blade performance. Finally, Computational Fluid Dynamic (CFD) is a good method for analyzing and verifying the performance of different types of blade shapes. For example, the National Aerospace Laboratory successfully developed a wind turbine with a 500 kW, low-cost, horizontal-axis, downwind, teetered and stall regulated two-bladed model using the CFD method to consider the optimum blade design and performance analysis [12]. Tachos, etc. [13] have used the Reynolds averaged Navier-Stokes equations combined with the k-ω SST turbulence model that describes the three dimensional (3D) steady state flow around the blade solved with the aid of a commercial CFD code for computing the aerodynamic characteristics of the NREL Phase VI rotor blade which is a horizontal-axis downwind turbine rotor [5,14].

2. Brief Description of the BEM Method:

The aerodynamic curves of the 2D airfoil are needed to analyze and combined these curves with the BEM theory to design the optimal blade shape. In this study, we obtained the NACA4418 airfoil data for BEM calculation by using the freeware XFoil from Massachusetts Institute of Technology [15]. From Figure 1, it can be seen that it is possible to obtain the distribution of the angle of relative wind (φ) which consists of pitch angle (θ_p), twist angle (β) and angle of attack (α) on one of the blade sections (airfoil) by employing BEM theory [1,2,6]. Figure 1 also shows the forces acting on an airfoil section, where TN is defined as the thrust and TQ is defined as the torque. Both are generated by lift (L) and drag (D) forces. The lift and drag are available as functions of the angle of attack and the Reynolds number (Re) which is defined as: where cavg. is the average chord length of each blade section; ρ is the air density; μ is the kinematic viscosity; and Vrel is the relative wind speed which consists of wind speed (V) and rotational speed (ω).
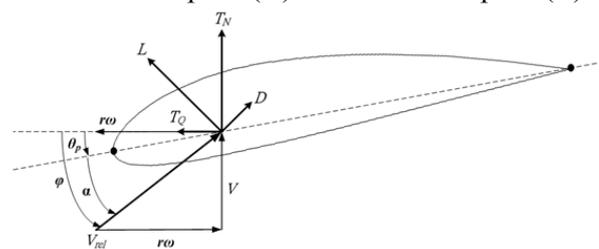
Figure 1. Diagram of angles and forces on one of the blade section

The blade shape used in this paper is a NACA4418 airfoils set with a design angle of attack (α_D) of 5.5°. Figure 2 shows the distribution of Reynolds numbers in each section at a wind speed of 10 m/s and tip speed ratio of 5 for the tested blade models used in the following content. We can see the distributions of Reynolds numbers of the OPT blade are between 8.0 × 104 and 1.1 × 105; there is very little difference in the

root region (r/R = 0.2–0.4) for the UOT and UUT blades. For this reason, a Reynolds number of 1.0 × 105 has been selected for the XFoil software calculation, which results in a lift coefficient (Cl) of 0.9005 and a lift to drag ratio (Cl/Cd) of 48. From Figure 2 it can be seen that the distributions of Reynolds number in the tested models are between 6.0 × 104 and 2.0 × 105 and the effect of the transition flow could occur in this case that caused from laminar to turbulence flow. The transition flow in XFoil relies on the en method, which has a user-specified parameter called the transition amplification ratio, Ncrit, which is the log of the amplification of the most-amplified frequency. Thus, the transition amplification ratio, Ncrit, has been set to 1 in XFoil [15] which was used in order to simulate both the effects of a wind tunnel free-stream turbulence intensity and blade surface roughness [15].
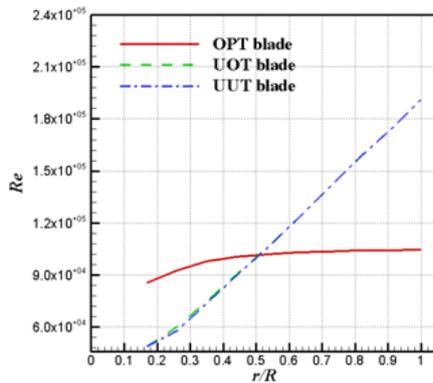
Figure 2. The distributions of Reynolds number in each section at V = 10 m/s and λ = 5.

where R is the radius of the blade. The test range of λ in this study is restricted between 2 and 9. In a steady state test, such as wind tunnel experiment, the distributions of angle of attack and Reynolds number can be changed with the various tip speed ratios, which will vary with the rotational speed. Figure 3 shows the distributions of angle of attack along each section at a wind speed of 10 m/s and tip speed ratios of 3, 5 and 7 for the tested models. Obviously, the distributions of angle of attack in each section between OPT and UOT blades completely overlap, because they have the same pitch angles but different chord length distributions in each section.

Because the rotational speed of the blade influences the Reynolds number, it is necessary to check its influence over this lift and drag. Figure 4 shows the results of a Reynolds number sensibility study made with XFoil over the performance of a NACA4418 airfoil at low Reynolds numbers when Ncrit = 1. These data can be used to improve the BEM model, design an OPT blade, and predict the blade performance, points which will be developed in the next section. Furthermore, these data also provide the numerical simulation of 2D airfoil in accordance with the results of the lift and drag coefficients that will be shown in detail in Section 4. The definition of power coefficient (Cp) for the blade can be written as: where Tm is the mechanical torque (N-m), which can be measured using a torque transducer during the wind tunnel experiment.
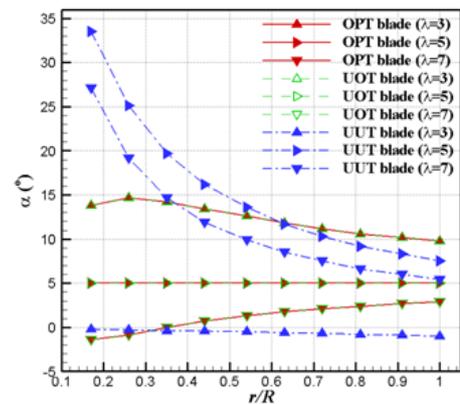
Figure 3. The distributions of angle of attack in each section at V = 10 m/s and λ = 3, 5 and 7.
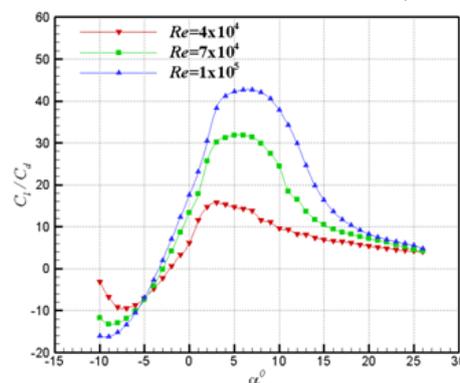
Figure 4. Airfoil data calculated from XFoil with Ncrit = 1.0 for the BEM predictions.

Improved BEM Method:

An airfoil has stall phenomenon when flow separates at high angles of attack, typically greater than 15°. Beyond this angle, the lift of the airfoil drops and drag increases significantly. To overcome this stall problem in the blade design, Viterna and Corrigan [16] have proposed a stall model which was successfully applied for predicting the lift and drag coefficients of a HAWT blade in the stall region. The rotational effect of the HAWT rotor blade is a typical case in which the so-called stall delay phenomenon occurs. This state is characterized by maintaining significant lift coefficient that is comparable with the 2D airfoil data measured in the wind tunnel with the occurrence of flow separation for the airfoil at a higher angle of attack beyond the stalled angle [17]. Even though this phenomenon was first observed in propeller blades [18], it has been applied to helicopters and we have even used our knowledge of this phenomenon (stall delay model) in wind turbine fields [2,6].

Because the pressure on the suction side of the blade is lower than on the pressure side, air tends to flow around the tip from the lower surface to the upper one and in this manner reduces both the lift together and the power production near the tip. This phenomenon is called tip-loss. In this study, the performance data of NACA4418 airfoil, calculated by XFoil at Reynolds number of 4×10^4, 7×10^4 and 1.0×10^5, were used in conjunction with the improved BEM model. The lift and drag coefficients were used to predict the blade performance with the angle of attack of less than 12°. When the angle of attack exceeds 12°, the VC stall model was performed to predict the performance of the blade in the stall region—the tip-loss factor and stall delay model were also combined with the improved BEM model to increase the accuracy of the performance prediction. All pertinent mathematical details can be found in [2,6].

3. Experimental Setup:

Three different HAWT blade models, shown in Figure 5, have been tested inside the wind tunnel.

The first one is the optimal (OPT) blade shape which was calculated by an in-house code developed using the improved BEM theory. It is composed of a NACA4418 airfoil that is tapered and twisted. Five parameters are needed to define a OPT blade shape design: (1) rated power; (2) rated wind speed; (3) design tip speed ratio; (4) number of blades; and (5) design angle of attack (Table 1). In this paper, the design angle of attack has been set to 5.5° because it generates the maximum lift to drag ratio when using a Reynolds number of 1.0×10^5 (Figure 4). All the design parameters are summarized in Table 2. The second blade model is an untapered and optimal twist (UOT) blade that has a constant chord of 0.055 m. The twist distribution is the same as the OPT. The blade radius is also 0.36 m and the NACA4418 airfoil was also used. The final one is an untapered and untwisted (UUT) blade that has the same parameters as the UOT blade, except the twist distribution is set to 0°.
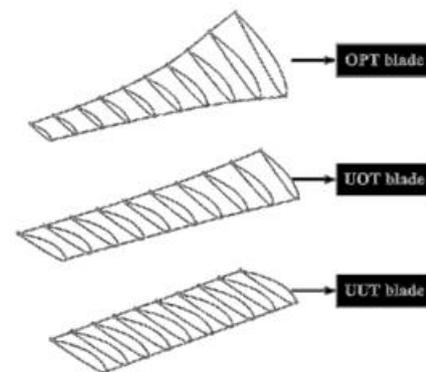
Figure 5. Three test blade models for wind tunnel experiment.

Table 1. The blade design parameters of OPT blade.

Design parameters	Values
Rated power (W)	50
Rated wind speed (m/s)	10
Design tip speed ratio	5
Number of blades	3
Design angle of attack (°)	5.5
Airfoil type	NACA4418

Table 2. Parameters of the OPT blade design.

Seconds	r/R	Airfoil type	Chord length (m)	Twist angle, β(°)
1	0.17	NACA4418	0.096	25.92
2	0.26	NACA4418	0.085	17.56
3	0.35	NACA4418	0.072	12.20
4	0.44	NACA4418	0.061	8.61
5	0.54	NACA4418	0.053	6.08
6	0.63	NACA4418	0.046	4.21
7	0.72	NACA4418	0.041	2.78
8	0.81	NACA4418	0.036	1.65
9	0.91	NACA4418	0.033	0.75
10	1.00	NACA4418	0.030	0.00

Figure 6 shows the results for the blades when tested inside the wind tunnel. The full scale wind tunnel experiment was used to provide the data for comparison with the BEM code. The test section of this wind tunnel is 1,440 mm long and the area of cross section is 1200 mm wide × 920 mm high. The specifications of the wind tunnel itself, which offers a maximum wind speed of 30 m/s, has been verified through many parameters including: structure vibration, temperature, stability, flow uniformity, turbulence intensity, flow angularity, and boundary layer thickness. The mean flow uniformity is about 0.37%, the turbulent intensity is less than 0.35% and the boundary layer thickness is about 60 mm at the inlet cross section. The flow angularity of pitch and yaw angles are, respectively, about ±0.415° and ±0.97° at a wind speed of 20 m/s. A pitot-static tube was adopted to measure the free stream velocity in the test section because it is stable, accurate and convenient to calibrate. A variable reluctance pressure transducer was connected to the pitot-static tube and transfers the pressure difference between the total pressure and the static pressure into electric voltage. The small analog signal was then amplified and converted using an analog/digital converter to digital dataflow and saved onto a personal computer (PC). The pressure transducer was calibrated using a micro manometer and certified. The flow speed in the test section was then calculated using the incompressible steady Bernoulli's equation [19].

(a)

(b)
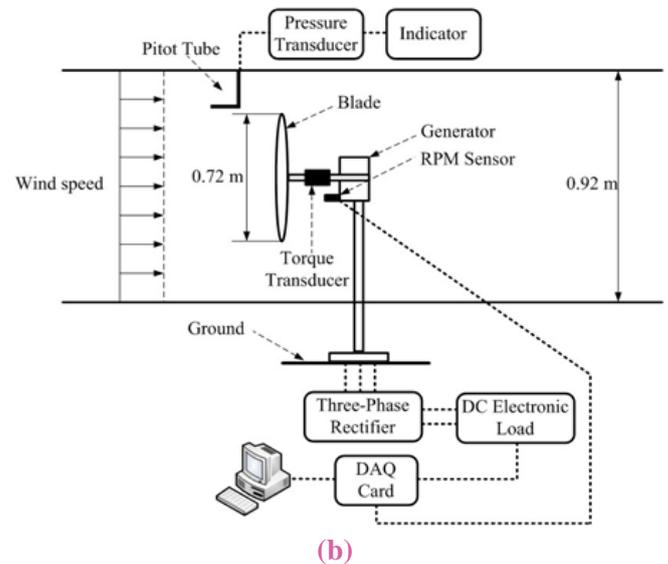
Figure 6. (a) The tested models setup inside the test section of full-scale wind tunnel; (b)The schematic of the tested models setup inside the test section of the full-scale wind tunnel.

In the wind tunnel experiments, the area ratio is defined as Ab/Aw, where Ab is the blade swept area and Aw is the cross section area of the wind tunnel test section. This area ratio is an index of the wind tunnel experiment for the HAWT system and allows us to have a maximum ratio of 30% without any interference effects from the wind tunnel wall on the power coefficient measurement, according to the reference [20]. In comparison with the area ratio of 8.8% for the NREL full-scale wind tunnel experiments performed using a blade with a radius of 5 m [21], in this study, the area ratio of the models is 36% and these models were tested in a closed test section. Obviously, our models are a little larger than the allowed maximum ratio, hence the blockage effect in the present study will also be a little higher. After our careful calculation and analysis, following the model of Barlow et al. [22], the blockage effect would be expected to cause a wind speed of 10 m/s, as an example, to be reduced by about 3% in the wind tunnel test. Therefore, the results of the power coefficient measurements with respect to the effective wind speed will also show an uncertainty (error) of 3% or less, which is still satisfactory in the experiments.
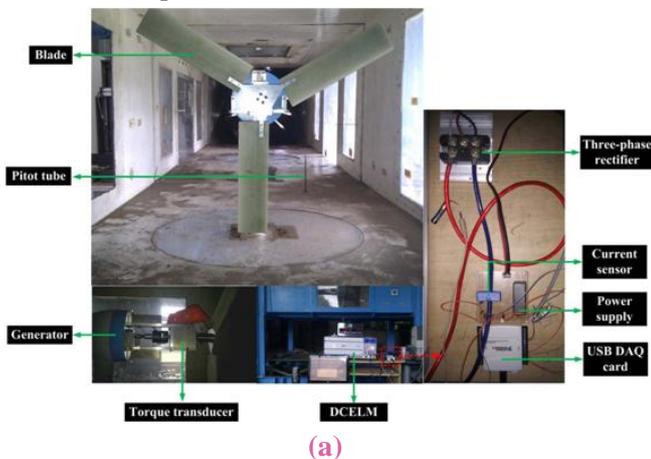
Furthermore, the Betz limit also indicates that as the rotor blade transports, the efficiency from wind energy (power coefficient) should have a maximum value of 59%. Our test results, shown in following section, do not exceed the Betz limit. In Figure 6 we can see the torque transducer used to measure the mechanical torque; it was mounted on the main shaft between the rotor blade and the generator. This measurement method, using a torque transducer for a HAWT blade, has been used by many authors [10,23], including as Kang et al. [23] who showed that the torque transducer can successfully measure the mechanical torque for power coefficient calculation. For the most accurate results, it is essential that the torque transducer be mounted as close as possible to the rotor blade to decrease any shaft frictional losses that might interfere with the measurement of the power coefficient.

The function of a high current DC electronic load module (DCELM) is to simulate the different loads of the circuit. If the circuit loads is changed by the DCELM, the rotational speed of the blade will also be changed. The operating region of the DCELM has four major functions: (1) constant current; (2) constant resistance; (3) constant voltage; and (4) constant power (between 0–60 V and 0–120 A). To be thorough, the signal of the rotational speed for the blade also needs to be measures. In this study a tachometer and proximity switch were used to measure the blades RPM. In this case, only the DC signal can be analyzed, so we used the simplest type of rectifier is a diode bridge circuit which converts the AC to fluctuating DC.

The acceptable input voltage of Analog/Digital converter is below 10 V. In order to measure higher voltages, the amount should be shrunk to one quarter. The current meter is an onboard function of the DC electronic load which directly converts the DC current into DC voltage and obtains the signal using an AD converter. The data acquisition for voltage outputs from these sensors were performed by National Instrument (NI) USB-6008 12 bit AD converter.

For the measurement of voltage, current and rotational speed in wind tunnel, the sampling frequency was fixed at 3 kHz and sampled at 6 k per point. The measuring time of data acquisition is 2 s. NI LabVIEW software was used to construct the data acquisition program.

4. Numerical Simulation:
4.1.2D Simulation:
The 2D calculations of the NACA4418 airfoil were performed using Fluent commercial software and the results have been compared to the XFoil software packages. Two fully turbulent models were used in the Fluent CFD simulation: the k-ω shear stress transport (SST) and the k-ε re-normalization group (RNG). A grid independency study was also performed to reduce the number of grid cells without losing accuracy. The high-resolution structured grids were used around the airfoil and unstructured grids were meshed in the outer domain. The study shows that a growth rate of 1.25 for the unstructured outer domain mesh could be used without significant loss of accuracy. Figure 7 show the grid independency study, including three turbulence models. It can be seen that the lift and drag coefficients have a great match compared with XFoil between y+ of 0.01 and 1. Thus, the first grid points next to the airfoil surface were set to 0.1 for all cases in this study, as required by the boundary layer calculation.
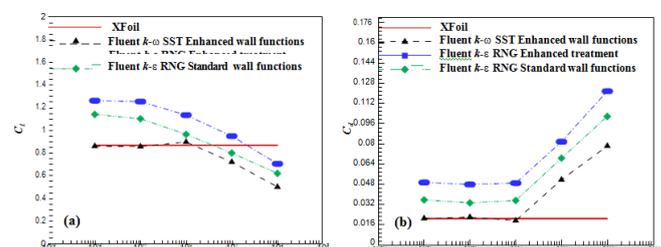
Figure 7. Lift and drag calculation check as a function of maximum y+ at the first grid where $\alpha = 5°$ and $Re = 1 \times 10^5$.

Figure 8 shows the various results of drag and lift obtained with Fluent and with XFoil at $Re = 1.0 \times 10^5$.

It can easily be seen that the k-ω SST turbulence model obtained the best agreement with the XFoil data, both for lift and drag coefficient prediction. On the other hand, the two k-ε turbulence models seem to over-predict the drag coefficient, and have a large error of almost 52%. The lift and drag coefficients of the wind tunnel measurement with Re = 2.5 × 105 [24] are also shown in Figure 8. It can be seen that there is a significant trend in the lift coefficient as the angle of attack is varied from −5° and 12°. Based on our findings, we are confident that the numerical simulation method works very well for completing the cases between the angle of attack of −5° and 12°.

It should also be noted that even though the lift coefficients between 13° and 20° from Fluent and XFoil have noticeable variation when compared with the data from the wind tunnel measurement, this discrepancy does not affect the results of this study because the VC stall model used in the stall region obtained excellent results. To sum up briefly, we designed the OPT blade at the angle of attack of 5.5° and used the VC stall model instead of the performance data of 2D airfoil at the stall region in the improved BEM model.
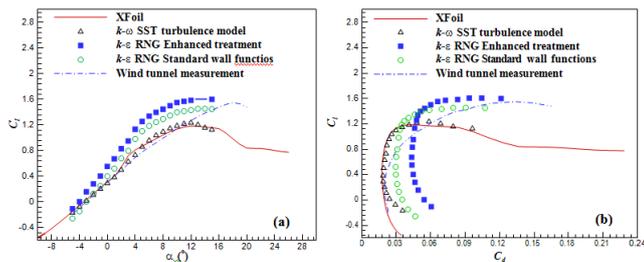
Figure 8. Comparison of lift and drag coefficients between XFoil and Fluent at Re = 1.0 × 105.

Having those results in mind, the choice of the k-ω SST turbulence model for the three-dimensional (3D) simulations becomes obvious. This choice is also supported by the recommendations of many authors [17,25].

4.2.3D Simulation:

A fair approximation for HAWT blade simulation is to neglect the hub, the tower and the ground in the computational domain. The simulation uses the moving reference frame (MRF) function of Fluent to simplify the problem that attached to the blade with the assumptions of incompressible and steady-state turbulent flow. The outer domain has a cylindrical shape with a radius equal to six times the blade radius measured from axial center, eight times the blade radius along the downwind direction and 1 radius lenght in the upwind direction. Exploiting the 120 degrees periodicity of the three-blades, it is possible to simplify the problem as shown in Figure 9.
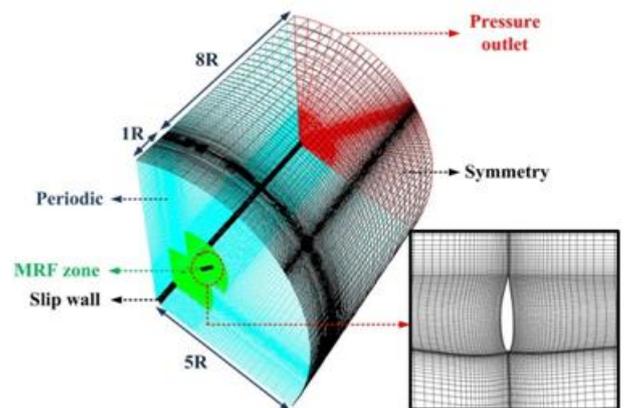
Figure 9. The mesh volume in 120 degrees section and definition of the boundary conditions and the H-type hexahedral mesh around the blade.

In this study, the Fluent's pre-processor Gambit was used to create a volume mesh, which is a hexahedral mesh of approximately 2.6 × 106 cells. As shown in Figure 9, an H-type grids has been used in order to resolve the boundary layer. Based on a 2D airfoil calculation, the first cell height has been set to keep the y+ values at 0.1 everywhere on the blade surface. All these calculations were carried out using an Intel Core 2 with 6 Gb RAM and the criterion of convergence was set to reduce the scaled residual below the value of 10−5. The inlet boundary condition of the domain was assumed to be uniform, with a wind speed of 10 m/s. The working fluid of the simulation is air with a constant density of 1.25 kg/m3.

The boundary condition for the outer cylinder is Euler-slip and for the inner one is symmetry. The blade surface is assumed to have a no-slip wall condition and the pressure outlet condition is assumed to be the extreme surface of the downwind field. All the boundary conditions can be seen in Figure 9. The calculation parameters have been adjusted to match changes in the experimental data, such as varying the rotational speed, which depends on the tip speed ratio of 2, 3, 4, 5, 6, and 7, where 5 is the design tip speed ratio.

5.Results and Discussion:

All the wind tunnel experiments were perfromed at constant wind speed of 10 m/s. The different tip speed ratios (λ) were obtained by adjusting the wind turbine's rotational speed. The mechanical torque, which is used to compute the power coefficient (Cp), was measured by averaging ten values of the torque transducer. Figure 10 shows the power coefficient distributions of the OPT, OUT and UUT blades at different tip speed ratios.
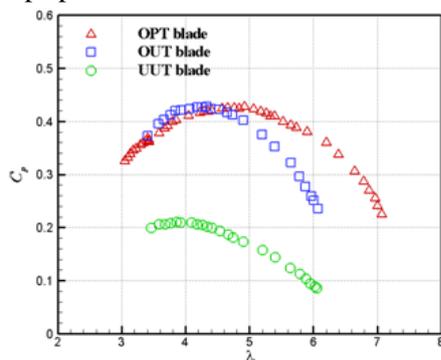
Figure 10. The experimental results of power coefficient as function of tip speed ratio for OPT, UOT and UUT blades at V = 10 m/s.

The OPT blade has a maximum power coefficient of Cp = 0.428 at λ = 4.92, which is very close to the design tip speed ratio, which is 5. It can be proven that the OPT blade conforms to the results of the BEM design. Unexpectedly, the UOT blade also obtained a maximum Cp value of 0.428, while the tip speed ratio is 4.32.

Although both the OPT and the OUT blades obtain an excellent power coefficient, we conclude that the OPT blade is better than the UOT blade because it has a higher range of high power coefficients. Indeed, even if the two blades have a similar power coefficient from a tip speed ratio of 3 to 5, the performances of the OUT blade quickly decreases after passing λ = 5 while the OPT blade keeps its high power coefficient until λ = 6. It can be understood from Figure 10 that the OPT blade operates quite well at high rotational speed. On the other hand, the UUT blade obtains its maximum power coefficient Cp = 0.210 at λ = 3.86, which is lower than for both the other blades. The main reason why Cp is so low is due to the stall phenomenon, which will be examined in more detail later.

The first calculations of power coefficient were undertaken using the in-house code which was developed using the BEM theory. All the settings used were set to correspond to the different cases discussed in this paper. The airfoil data, function of the Reynolds number (Re) given by XFoil have been combined into the code. We developed to compute the power coefficient of tip speed ratios from 0 to 9. This means that the operational range of the NACA4418 used would be from angle of attack −5 to 55, but from Figure 4 it can be clearly seen that we only have the data for angles of attack from −10 to 28. Here the Viterna-Corrigan stall model [13] was combined with our code to successfully predict the blade performance both near the stall region and after the stall point.

Figure 11 show the power coefficient comparison as a function of the tip speed ratio for the OPT, the UOT and the UUT blades. However the predictions made using the improved BEM method and CFD simulation have a good trend of power coefficient curves when compared with the experimental data. The BEM method uses some correction factors such as tip loss and rotational augmentation, and these have been included in our in-house code. When the turbine blade was operated at a tip speed ratio of less than 3, the distributions of angle of attack was always greater than 20° and the significant stall effects are occurred at

whole blade section for these three blades. This solution is quite good for predicting Cp for low tip speed ratios. Also, we determined that the Viterna-Corrigan stall model is available for this BEM code. Though the BEM method predicts a good trend for higher tip speed ratios ($\lambda > 5$), the Cp values clearly over-predict after $\lambda = 5$ for these blades. The small differences between the BEM and CFD predict Cp at high tip speed ratios ($\lambda > 5$) probably come from the difference in boundary layer development and particularly related to whether or not the flow is turbulent from the leading edge. Indeed, this phenomenon of boundary layer development is not mathematically compatible with the BEM code. However, this could be an indication that the 2D airfoil data used from XFoil are available for a high angle of attack.

The CFD simulation method gives similar results to the experimental data for all three blade models, and is particularly good at identifying the maximum point of Cp, which comes out the same for all three. This conclusion strongly supports the fact that we can use the CFD simulation to further numerically observe the pressure distribution and the flow fields along the spanwise direction of the blade. Figure 12 shows the sectional pressure fields of different radial sections for the OPT, the UOT and the UUT blades. Several things should be noticed. First of all, it can be seen that there is almost no pressure difference at the blade roots (r = 0.060 m) for $\lambda = 3$, 5, and 7. Similarly, we find that the OPT and the UOT blades have almost the same pressure difference at r = 0.193 m for $\lambda = 3$ and $\lambda = 5$ while the UUT blade has a larger pressure difference.

The larger difference of the pressure for these three blades is at around the two-thirds mark (r = 0.327 m). Also, in comparing the upper and lower surfaces at $\lambda = 7$ for these blades, we see that the OPT blade has a slightly larger low-pressure area than other two, which may be why more power is predicted for the OPT blade, a result which explains why the OPT blade produces more Cp value than other two blades in the experimental results.

From the experimental data (Figure 10), the Cp value of the OPT blade is slightly larger than the UOT blade and a fair amount larger than the UUT blade at $\lambda = 5$, which is the design tip speed ratio. The differences in the OPT and UOT blades can be observed in the CFD simulation shown as Figure 12b, in which the pressure distribution is almost the same at r = 0.060 m and r = 0.193 m and there is a slight difference at r = 0.327 m.
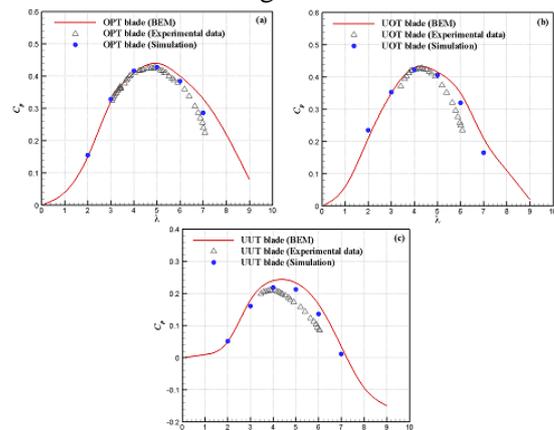
Figure 11. (a) Power coefficient calculated for OPT blade using BEM and simulation methods as compared with experimental data; (b) Power coefficient calculated for UOT blade using BEM and simulation methods as compared with experimental data; (c) Power coefficient calculated for UUT blade using BEM and simulation methods as compared with experimental data.

(a)

(b)
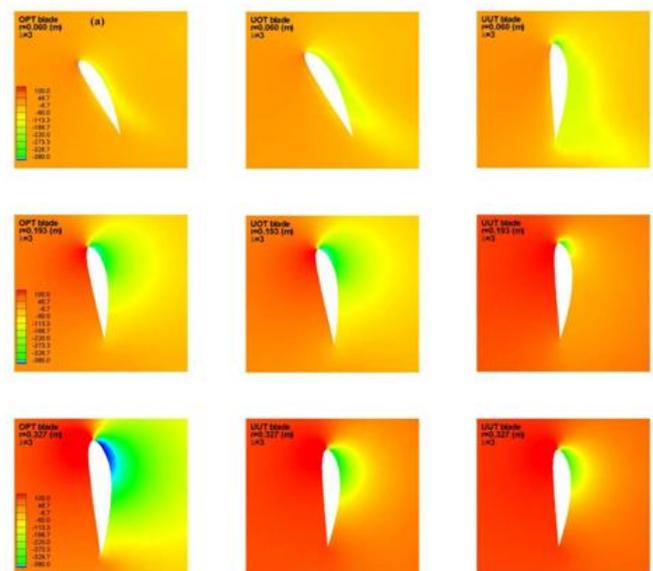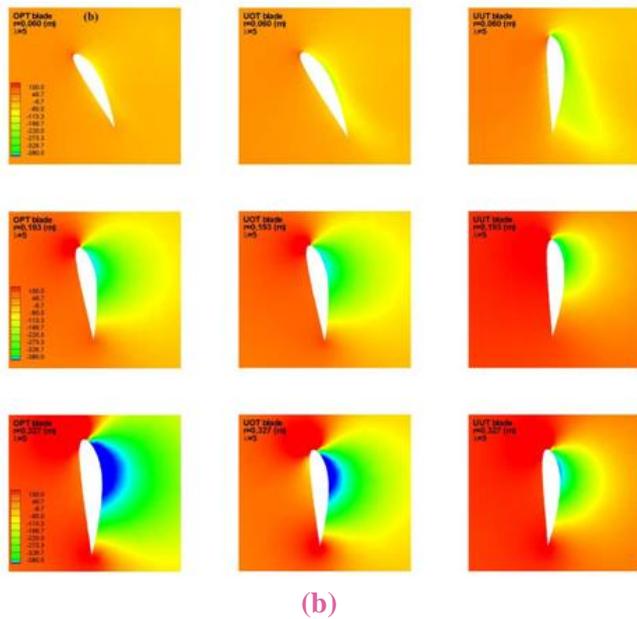
Figure 12. (a) The distributions of the pressure field for OPT, UOT and UUT blades in r = 0.060 (m), r = 0.193 (m) and r = 0.327 (m) at V = 10 (m/s) and λ = 3; (b) λ = 5; (c) and λ = 7.

(c)
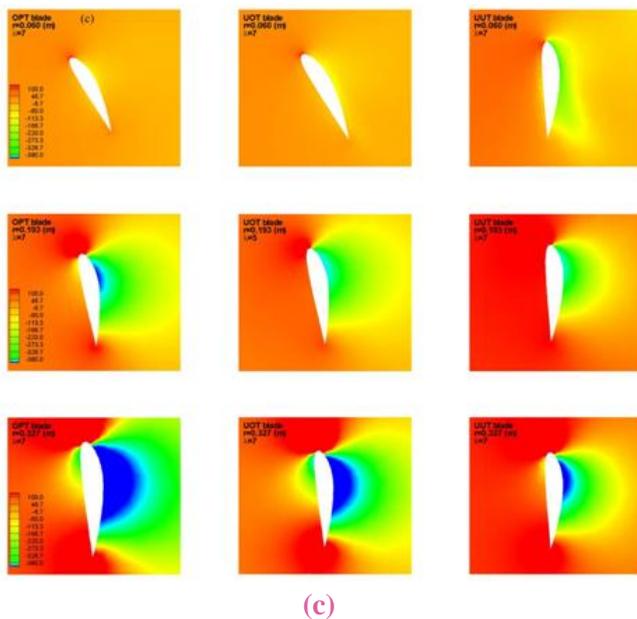
Figure 12. Cont.

Figure 13a–c shows the vector plots at 54% of the span of the OPT, the UOT and the UUT blades at λ = 3 and V = 10 m/s. It is clear that the UUT blade suffers from a deep stall phenomenon over the entire suction surface, mainly because the operating angle of attack

is about 21°. This phenomenon partially explains why the power coefficient of the UUT blade is lower than the OPT and the UOT blades. As expected, the vector plots for the OPT and the UOT blades at λ = 5, which is the design tip speed ratio, show that the flow behaves well as shown in Figures 13e,f. It should be noted that though the flow is good at λ = 7 for these three blades, the maximum lift to drag (Cl/Cd) ratio of λ = 5 is 42, which is larger than λ = 7 (Cl/Cd = 23). Consequently, the OPT blade obtains its best power coefficient (0.428 from the experimental data) at λ = 5. The rotational effect of the HAWT rotor blade can lead to the so-called stall delay phenomenon, which is characterized by maintaining a significant lift coefficient. This situation is like the corresponding two-dimensional (2D) airfoil data measured in a wind tunnel in which the flow separation for the airfoil is at a higher angle of attack, beyond the stalled angle. Although the angle of attack is greater than 12° in 54% span at λ = 5 for the UUT blade, Figure 13d implies that the flow is still appropriate and the lift coefficient is 1.933. Figure 13e,f also show that the UOT and OPT blades have a healthy flow with an angle of attack of 5° in 54% span at λ = 5. The lift coefficients for these are 1.922 for the UOT blade and 1.936 for the OPT blade. These results were calculated using a Fluent k-ω SST turbulence model.
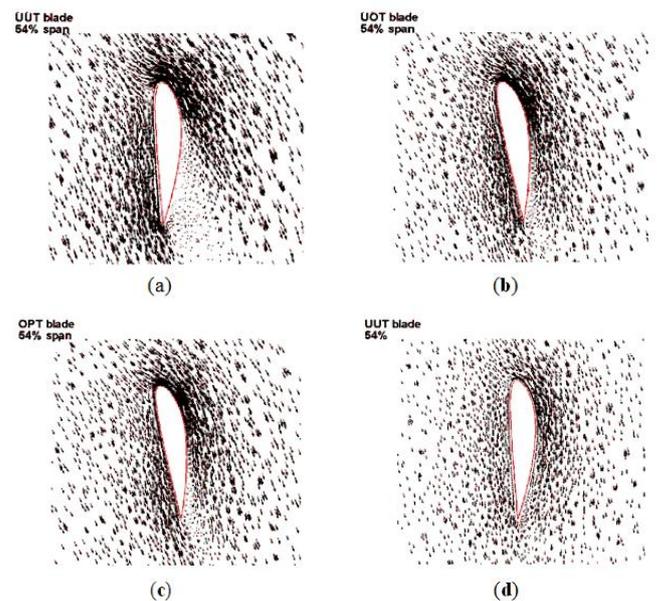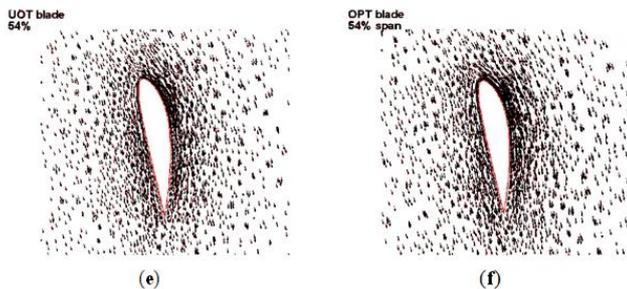
Figure 13. (a) The vector plots of flow field for UUT blade in 54% at V = 10 (m/s) and λ = 3; (b)The vector plots of flow field for UOT blade in 54% at V = 10 (m/s) and λ = 3; (c) The vector plots of flow field for OPT blade in 54% at V = 10 (m/s) and λ = 3; (d) The vector plots of flow field for UUT blade in 54% at V = 10 (m/s) and λ = 5; (e) The vector plots of the flow field for the UOT blade in 54% at V = 10 (m/s) and λ = 5; (f) The vector plots of flow field for OPT blade in 54% at V = 10 (m/s) and λ = 5.

6. Conclusions:

The wind tunnel test results presented in this paper show that the OPT and the UOT blades obtain the same maximum power coefficient (Cp = 0.428) but at different tip speed ratio points. However, we conclude that the OPT blade is better than the UOT blade because its measured power coefficient is higher over a wider range of tip speed ratios, which go from 4.5 to 7. The UUT blade obtains the lowest Cp value because it almost always operates in stall conditions, indicating that the optimal design for the blade shape using the BEM method is needed, especially in the distribution of twist and chord length along the direction of the blade, spanwise. This paper also shows that the in-house code, which uses the BEM theory, is useful not only for designing the optimal blade shape but also at predicting the blade performance. This review has also shown that XFoil is a good tool for predicting the lift coefficient, although in our test it tended to underestimate the drag coefficient a bit. This is shown in the CFD simulations using the commercial code Fluent, which consistently computed the same lift coefficients but higher drag coefficients.

Detailed flow fields were also investigated using full 3D CFD simulations by means of the commercial code Fluent and the k-ω SST turbulence model. The good agreement between the power coefficient computed by the Fluent package and the experimental data has been used in the validation process where it indicates that the Fluent package can be used to successfully predict the performances of a wind turbine.

References:

1. Manwell, A.; McGowan, J.G.; Rogers, A.L. Wind Energy Explained—Theory, Design and Application, 2nd ed.; John Wiley & Sons Ltd.: West Sussex, UK, 2010; pp. 83–134.

2. Bai, C.J.; Hsiao, F.B. Using CFD Computation for Aerodynamic Performance Design and Analysis of Horizontal Axis Wind Turbine Blade. In Proceedings of the 15th National Computational Fluid Dynamics Conference, Tainan, Taiwan, 7–9 August 2008.

3. Schreck, S. The NREL full-scale wind tunnel experiment introduction to the special issue. Wind Energy 2002, 5, 77–84.

4. Johansen, J.; Srensen, N.N.; Michelsen, J.A.; Schreck, S. Detach-eddy simulation of flow around the NREL phase VI blade. Wind Energy 2002, 5, 185–197.

5. Srensen, N.N.; Michelsen, J.A.; Schreck, S. Navier-stokes predictions of the NREL phase VI rotor in the NASA ames 80 ft × 120 ft wind tunnel. Wind Energy 2002, 5, 151–169.

6. Bai, C.J.; Hsiao, F.B. Code Development for Predicting the Aerodynamic Performance of a HAWT Blade with Variable-Operation and Verification by Numerical Simulation. In Proceedings of the 17th National Computational Fluid Dynamics Conference, Taoyuan, Taiwan, 29–31 July 2010.

7. Glauert, H. The Elements of Aerofoil and Airscream Theory, 2rd ed.; Cambridge University Press: Cambridge, UK, 1948.

8. Madsen, H.; Christensen, H. On the relative importance of rotational, unsteady and three-dimensional effects on the HAWT rotor aerodynamics. Wind Eng. 1990, 4, 405–415.

9. Narramore, J.C.; Vermeland, R. Navier-stokes calculations of inboard stall delay due to rotation. J. Aircr. 1992, 29, 73–78.

10. Hirahara, H.; Hossain, M.Z.; Kawahashi, M.; Nonomura, Y. Testing basic performance of a very small wind turbine designed for multi-purpose. Renew. Energy 2005, 30, 1279–1297.

11. Koki, K.; Taniguchi, H.; Suzuki, J.; Ibano, H.; Kakashi, K.; Turuhami, M. Theoretical and experimental study on the aerodynamic characteristics of a horizontal axis wind turbine. Energy 2005, 30, 2089–2100.

12. Sajjan, S.V.; Savanur, R.A.; Mudkavi, V.Y. CFD Analysis of 500 kW Horizontal-Axis Wind Turbine Blades: Straight and Bent Cases. In Proceedings of 11th Annual CFD Symposium, Bangalore, India, 11–12 August 2009.

13. Tachos, N.S.; Filios, A.E.; Margaris, D.P.; Kaldellis, J.K. A computational aerodynamics simulation of the NREL phase II rotor. Open Mach. Eng. J. 2009, 3, 9–16.

14. Potsdam, M.A.; Mavriplis, D.J. Unstructured Mesh CFD Aerodynamic Analysis of the NREL Phase VI Rotor. In Proceedings of 47th AIAA Aerospace Sciences Meeting, Orlando, FL, USA, 5–8 January 2009.

15. Drela, M. XFOIL: An Analysis and Design System for Low Reynolds Number Airfoils. In Proceedings of Low Reynolds Number Aerodynamics, Notre Dame, IN, USA, 5–7 June 1989.

16. Viterna, L.A.; Corrigan, R.D. Fixed Pitch Rotor Performance of Large Horizontal Axis Wind Turbines. In Proceedings of DOE/NASA Workshop on Large Horizontal Axis Wind Turbine, Cleveland, OH, USA, 29–30 July 1981; pp. 69–85.

17. Dumitrescu, H.; Cardos, V. Rotational effects on the boundary-layer flow in wind turbines. AIAA J. 2003, 42, 408–411.

18. Glauert, H.; Division, L. Airplane Propellers. In Aerodynamic Theory; Durand, W.F., Ed.; Springer: Berlin, Germany, 2007; Volume 4, pp. 169–360.

19. Liu, Y.C.; Hsiao, F.B. Aerodynamic investigations of low-aspect-ratio thin plate wings at low reynolds numbers. J. Mech. 2012, 28, 77–89.

20. Spera, D.A. Wind Turbine Technology: Fundamental Concepts of Wind Turbine Engineering; ASME Press: New York, NY, USA, 1994.

21. Simms, D.; Schreck, S.; Hand, M.; Fingersh, L.J. NREL Unsteady Aerodynamics Experiment in the NASA-Ames Wind Tunnel: Comparison of Predictions to Measurements; NREL/TP-500-29494; National Renewable Energy Laboratory (NREL): Golden, CO, USA, 2001.

22. Barlow, J.B.; RAE, W.H.; Pope, A. Low-Speed Wind Tunnel Testing, 3rd ed.; Wiley-Interscience: New York, NY, US, 1999; pp. 328–441.

23. Kang, H.S.; Meneveau, C. Direct mechanical torque sensor for model wind turbines. Meas. Sci. Technol. 2010, 21, doi: 10.1088/0957-0233/21/10/105206.

24. Ostowari, C.; Naik, D. Post-Stall Wind Tunnel Data for NACA 44xx Series Airfoil Sections; A

Subcontract Report; Solar Energy Research Institute: Golden, CO, USA, 1985; pp. 21–25.

25.Hansen, M.O.L.; Sørensen, J.N.; Voutsinas, S.; Sørensen, N.N.; Madsen, H.A. State of the art in wind turbine aerodynamics and aeroelasticity. Prog. Aerosp. Sci. 2006, 42, 285–330.